2015 IEEE International Conference on Robotics and Automation (ICRA)
Washington State Convention Center
Seattle, Washington, May 26-30, 2015

Limbless Locomotors that Turn in Place

Chaohui Gong, Matthew Travers, Henry C. Astley, Daniel I. Goldman and Howie Choset

***Abstract*— Our research group has started a collaboration that analyzes data collected from biological snakes to provide insight on how to better program snake robots. Most data collected on biological snakes views the snakes from above and thus can only detect motion in the horizontal plane. However, both our robots and biological snakes are capable of generating motions both in the horizontal and vertical planes. Vertical waves naturally play a major role in limbless locomotion in that they simultaneously provide thrust motion and make-and-break contact between the mechanism and environment. Analysis on the data, collected from sidewinder rattle snakes, revealed that disparate modes of locomotion emerged from different contact patterns. We conclude that the same horizontal undulation can cause dramatically different motions for both the biological and robotic snakes depending upon the choice of contacts. With this knowledge, we introduce contact scheduling, a technique that plans positions of contacts along the body to design gaits for snake robots. Contact scheduling results in a novel turning gait, which can reorient a snake robot more than 90 degrees in one gait cycle.**

I. Introduction

Sidewinder rattlesnakes locomote via three-dimensional body undulations [1] which can be modeled as a combination of two waves in the horizontal and vertical planes [2]. Naturally, the motions of both waves play a critical role in the overall motion of the snake and robot. To highlight the role of the vertical wave, we noted that biological snakes were able to perform different types of motion with similar horizontal undulations, as shown in Fig. 1(a). These qualitatively different motions resulted from the different ways snakes actuated their body in the vertical direction. Studying how animals utilized vertical motion (and contacts) to generate versatile behaviors would lead to the discovery of general locomotion principles that can guide motion designs for robots.

Horizontal motion has been well studied in understanding the motion of snakes, but how vertical motion alter the form of locomotion is largely an unexplored area (see [3]). Vertical motion is known to be useful for redistributing body weight [4] and regulating the length of body contact segments [2], but the mechanism by which it changes the mode of locomotion was not well understood. Vertical waves determined the locations of contacts and where along the body to interact with the environment. Therefore, we hypothesized that diverse modes of locomotion can be generated by varying where (along the body) and when to contact the ground for both biological and robotic locomotion.

We collected motion capture data from sidewinder rattlesnakes, *Crotalus cerastes*. Distinct *contact patterns*, sequences that describe where and when contacts were made between the snake and the environment, were observed from

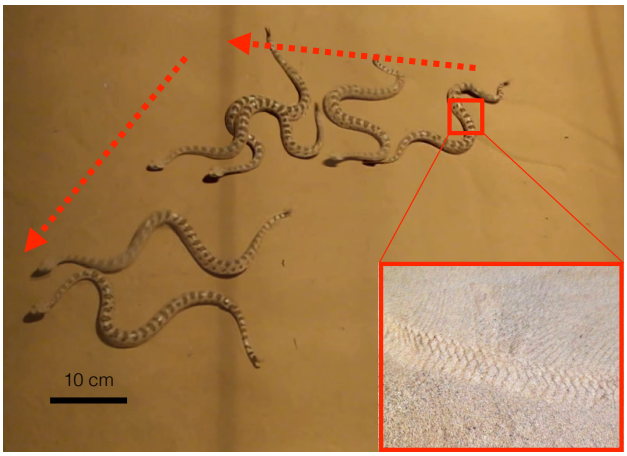

(a) The trajectory of a sidewinder rattlesnake (See supplementary video).

(b) The trajectory of a snake robot (See supplementary video).

Fig. 1: A comparison between the workspace trajectory of a biological snake and a snake robot. The red arrows indicate the direction of motion.

different modes of snake motions. To study the mechanics of how contact patterns impact locomotion, we derived a mechanical model (a numerical simulator) of a sidewinding snake. This model revealed that the horizontal undulation and the positions of contacts together determined the resultant motion. With this understanding, we introduce the *contact scheduling* algorithm which designs gaits by planning contact patterns. In contrast to intrinsic trajectory generation techniques [5], contact scheduling is a model-based approach. Applying contact scheduling to snake robots resulted in a novel type of turning motion, which was more agile than turning gaits that have been previously implemented on snake robots [6]–[8]. This turning motion was enabled by switching the positions of body contacts, a mechanism different from turning motions in swimming [9] and slithering [8].

978-1-4799-6922-7/15/$31.00 ©2015 IEEE

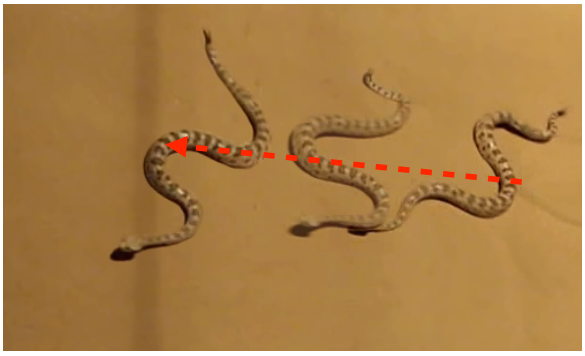

(a) Straight-line sidewinding.

(b) Turn in place.

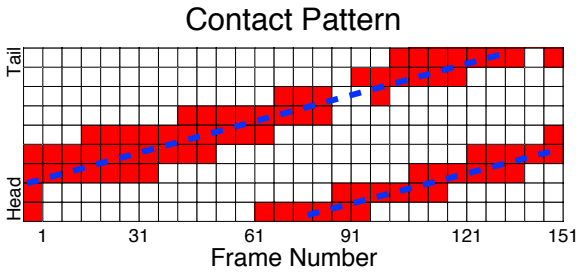

(c) Contact pattern of straight-line sidewinding.

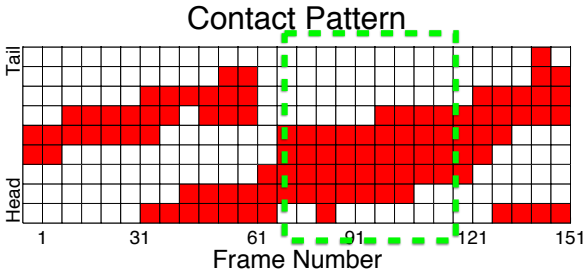

(d) Contact pattern of turn in place.

Fig. 2: Contact patterns of different modes of snake locomotion. The color of every square in (c) and (d) represents whether a particular body segment at a particular time instance is in contact or not. Red means a body segment in contact, and white means a lifted body segment. The blue dashed lines in Fig. 2(c) show that the contact pattern emerged from sidewinding along a straight line. The green dashed box in Fig. 2(d) highlights a contact pattern different from that of straight-line sidewinding.

II. Observation of Biological Snakes

Sidewinding is a gait composed of both in-plane (horizontal) and out-of-plane (vertical) body undulations [10]. We observed that sidewinder rattlesnakes displayed distinct modes of locomotion even with similar horizontal undulations. We therefore hypothesized that the snakes utilized vertical waves to alter the positions of contacts to achieve distinct behaviors. Analysis of the contact patterns supported our hypothesis.

A. Distinct Modes of Locomotion

As shown in Fig. 1(a) (and supplementary video), sidewinder rattlesnakes changed from sidewinding along a straight path to a rapid *turn in place* motion (the reorientation phase of a *reversal turn* using the terminology in [11]) and then switched back to straight sidewinding without noticeable disruption in body undulations. In less than 0.5 seconds, the snake reoriented more than 90 degrees. This turn in place motion presented an exceptional level of maneuverability (small turning radius) and agility (large angular velocity), superior to any gait that has been implemented on snake robots [6], [7], [12].

Before, during and after the turn in place motion, no apparent discontinuity of horizontal body undulation was observed, but the reorientation was rapid and significant. We hypothesized that the snakes manipulated the positions of contacts along its body (via vertical undulation) to produce different modes of locomotions.

B. Contact Detection

To investigate the impact of altering the positions of contacts, we used motion capture data collected from the biological snakes to first infer contacts and then study their relation to the resulting motions.

1) Snakes and System: The research subjects were four adult sidewinder rattlesnakes, *Crotalus cerastes* ($m = 98 \pm 18\ g, L = 48 \pm 6\ cm$), collected near Yuma, AZ (under appoval GT IACUC A11053). The tests were conducted in a $1m \times 2m$ fluidization bed, filled with natural sand. Four OptiTrack Flex 13 cameras (Natural Point, Inc.) operating at 120 FPS, were used to track the 3D positions of 10 reflective markers pasted along the snakes. Before each trial, the sand was fluidized to a loosely packed state to ensure consistent initial conditions of the test environment over all animal trials [13].

2) Contact Detection: Though the motion capture system measures the 3D positions of the reflective markers, due to the fact that biological snakes sidewind with small ground clearance, less than the precision of the camera system, it was unreliable to directly use Z-measurements to infer contacts or vertical motion. Based on the key property that sidewinding snakes make static contacts with the substrate [1], [10], [14] (also see Fig. 1(a)), it can be deduced that the body segments in contact with the ground should have small instantaneous velocities. We hence labeled a marker and its corresponding body segment as being in contact if its instantaneous velocity, the spatial displacement between two video frames, was less

than or equal to 1 mm (twice the tolerance of the motion capture system to avoid missing a true contact because of the system errors). We remark that this contact detection method could produce false-positives (label a lifted segment as being in contact) in case a snake moves at extreme low speed, but it is unlikely to miss an actual contact.

C. Contact Pattern Extraction

Using the contact detection method, we obtained the contact patterns, sequences describing where and when contact is made between the snakes and the environment, of both straight-line sidewinding (Fig. 2(c)) and the turn in place motion (Fig. 2(d)). While the undulatory patterns in the horizontal plane were similar, the contact pattern of the turn in place motion differed qualitatively from that of straight-line sidewinding, as shown in Fig. 2.

1) Straight Sidewinding: The contact pattern of straight sidewinding emerged a traveling wave pattern, highlighted by the blue dashed lines in Fig. 2(c). During straight sidewinding, the snakes made contacts at discrete portions along the body. As the motion proceeded, the positions of contacts progressively shifted from head to tail at an almost uniform speed. This pattern was also reported in biology literature [1], [14].

2) Turn in Place: The contact pattern of the turn in place motion differed from that of straight sidewinding, especially in the region highlighted by the green dashed box in Fig. 2(d). The contact patterns outside the green box were more or less similar to that of straight sidewinding. However, in the green box, the middle portions of the snake (from marker 2 to 6) were in complete contact with the substrate, showing a pattern different from that of straight sidewinding.

III. Modeling Snake Locomotion with Switching Contacts

The qualitatively different contact patterns between straight sidewinding and the turn in place motion suggested contact patterns were indeed the key to the generation of different modes of locomotions. To further investigate the mechanism by which contacts impact limbless locomotion, we derived a mathematical model (a numerical simulator) of a sidewinding snake. To emulate the vertical wave, we assumed that each link can make and break contact with the environment on command. This assumption simplified mathematical modeling of contacts but will be relaxed in Sec. V.

A. N-Link Snake Model

The derivation of the N-link snake model was based upon the characteristics of the contacts that sidewinders make: these contacts are static, similar to a wheel rolling on the ground. First, as discussed in [15], because sidewinders move by "laying down" and "peeling off" body segments, different choices of friction model would lead to identical results. We hence used viscous friction model in our formulation for simplicity. Second, sidewinders locomote with minimal slip: their motions are dominated by friction and any inertial/dynamic effect is immediately dissipated. These two characteristics are reminiscent of the two fundamental assumptions for systems swimming in low Reynolds number fluid [16]: 1) the resistive force of a rigid body is proportional to its body velocity (viscosity assumption) and 2) the total net forces experienced by a system sum to zero (dynamic dissipation). Therefore, leveraging modeling tools from fluid mechanics [17], we modeled a sidewinding snake in a way similar to a low-Reynolds number swimmer, but with a modification to account for the contacts.

The body velocity of link i with respect to the head frame (link 0) was denoted as ξ_{0i} and was computed using the differential mapping,

$$\xi_{0i} = \mathbf{J}_i^b \begin{bmatrix} \dot{\alpha_1} & \cdots & \dot{\alpha_i} \end{bmatrix}', \tag{1}$$

where $J_i^b \in \mathbb{R}^{3\times i}$ was the body Jacobian when viewing link i as the tool frame [18] and α denoted the internal joint angles (shape variables). To facilitate further derivation, we rewrote (1) into the following,

$$\xi_{0i} = \begin{bmatrix} \mathbf{J}_i^b & \mathbf{0}_i \end{bmatrix} \dot{\alpha} = \mathbf{J}_i \dot{\alpha}, \tag{2}$$

where $\mathbf{0}_i \in \mathbb{R}^{3\times(N-i)}$ denoted a matrix filled with zeros and $\mathbf{J}_i \in \mathbb{R}^{3\times N}$ was a linear differential map from joint velocity (shape velocity) $\dot{\alpha}$ to ξ_{0i}. We denoted the body velocity of the head with respect to the world frame as ξ_{w0}. The body velocity of individual links with respect to the world frame was then computed using the following [18],

$$\xi_{wi} = \mathrm{Ad}_{g_{0i}^{-1}} \xi_{w0} + \xi_{0i}, \tag{3}$$

where Ad_g denoted the adjoint operator, which maps body velocity between different frames. To encode contacts, we introduced a binary vector, called the *contact state*,

$$\delta = \begin{bmatrix} \delta_0 \\ \vdots \\ \delta_N \end{bmatrix}, \tag{4}$$

where $\delta_i = 1$ denoted link i was in contact with the ground and vice versa. The viscous force experienced by link i with respect to its own body frame was thus computed as

$$F_i^b = -\delta_i \mathbf{K} \xi_{wi} = -\delta_i \begin{bmatrix} k_x & & \\ & k_y & \\ & & k_\theta \end{bmatrix} \xi_{wi}, \tag{5}$$

where $k_x = k_y = k_\theta = 1$. F_i^b was then transformed in the head frame using the following [18],

$$F_i = \mathrm{Ad}_{g_{0i}}^{'} F_i^b \tag{6}$$

where F_i denoted the force applied to link i with respect to the head frame. The low Reynolds number assumption implied that all the dynamic effects were dissipated during locomotion. Therefore, the net forces experienced by the system summed to zero [17],

$$\sum_{i=0}^{N} F_i = \mathbf{0}. \tag{7}$$

Rewriting (7) in terms of $\dot{\alpha}$ and ξ_{w0} led to

$$\sum_{i=0}^{N} \left(\delta_i \mathrm{Ad}'_{g_{oi}} \mathbf{K} \left(\mathrm{Ad}_{g_{oi}^{-1}} \xi_{w0} + \mathbf{J}_i \dot{\alpha} \right) \right) = \mathbf{0}. \tag{8}$$

A close inspection of (8) showed that the only unknown variable was the body velocity of the head frame, ξ_{w0}. Further manipulation of (8) resulted in the following,

$$\underbrace{\left(\sum_{i=0}^{N} \left(\delta_i \mathrm{Ad}'_{g_{oi}} \mathbf{K} \mathrm{Ad}_{g_{oi}^{-1}} \right) \right)}_{\omega_\xi} \xi_{w0} = - \underbrace{\sum_{i=0}^{N} \left(\delta_i \mathrm{Ad}'_{g_{oi}} \mathbf{K} \mathbf{J}_i \right)}_{\omega_\alpha} \dot{\alpha}.$$

The body velocity of the head frame, ξ_{w0}, was then computed as

$$\xi_{w0} = -\omega_\xi^{-1} \omega_\alpha \dot{\alpha} = \mathbb{A}(\alpha, \delta) \dot{\alpha}, \tag{9}$$

which was determined by instantaneous shape changes, $\dot{\alpha}$, as well as contact state, δ.

In case there is no contact, ω_ξ is singular and not invertible. To guarantee numerical stability, we rewrote (9) as

$$\xi_{w0} = -\omega_\xi^{\dagger} \omega_\alpha \dot{\alpha} \tag{10}$$

where $\omega_\xi^{\dagger}$ was the *singularity robust inverse* defined as in [19],

$$\omega_\xi^{\dagger} = \left(\omega_\xi' \omega_\xi + \lambda I \right)^{-1} \omega_\xi', \tag{11}$$

and $\lambda = 1$.

Equation (10) was used to simulate the snake motions. A gait cycle was first discretized into T time steps ($T-1$ time intervals). In each time interval, the contact state, δ, was determined using the contact detection method described in the previous section. When the marker i was labeled as in contact, we set $\delta_i = 1$. Otherwise, $\delta_i = 0$. To retrieve the internal joint angles, α, we represented the biological snakes as comprised of 9 rigid links, each of which was determined by connecting two adjacent markers. We then computed α as the relative angles between neighboring links, as shown in Fig. 3(a). Finally, the shape velocities, $\dot{\alpha}$, were computed by numerically differentiating α using the forward difference rule. After obtaining $\dot{\alpha}$ and δ from the biological data, we calculated the instantaneous body velocity of the head frame at the beginning of every time interval using (10). During every time interval, a constant body velocity was assumed and, as a result, the configuration of the head frame after one time step was updated by right multiplying a homogeneous transformation [18],

$$h = \exp(\hat{\xi}_{w0} \Delta t). \tag{12}$$

It must be noted that the workspace motion of the entire snake is invariant to the particular choice of body frame (head frame in this case) because the workspace motion is solely determined by contacts and shape velocity.

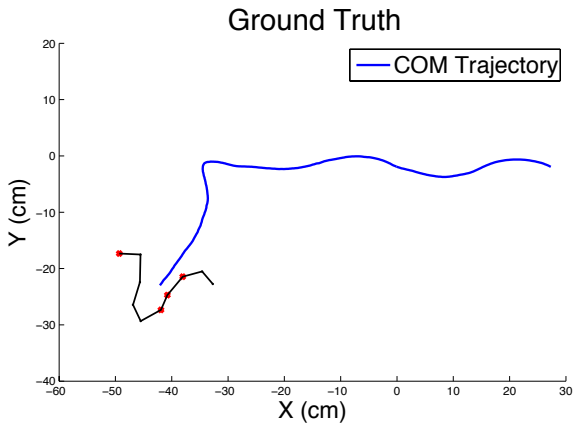

(a) CoM trajectory determined from the snake motion capture data.

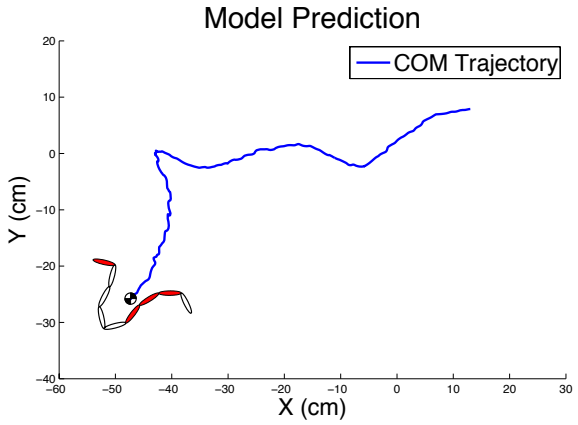

(b) Model predicted CoM trajectory.

Fig. 3: A comparison between the CoM trajectory (approximated as the average joint position) of a biological snake and that predicted by the mathematical model using the same body undulations and contacts. A segment in red denotes it is in contact with the ground.

B. Model Evaluation

We next verified the accuracy of (12) in modeling biological snake motions. We input $\dot{\alpha}$ and δ determined from biological data to the model and then compared the model-predicted results with the actual animal motions. Fig. 3 shows one comparison of the CoM trajectories (average position of the joints/markers) between the model-predicted results versus actual motion capture data (the same data set as shown in Fig. 1(a)). Despite the discrepancies in many details between the model and the snakes, the motion predicted by the model closely matched with the actual animal motion. Results of similar qualities were obtained on the other 19 data sequences.

The verified efficacy of the snake model led to two key conclusions. First, these results showed that positions of contacts are crucial in three-dimensional terrestrial limbless locomotion and a variety of behaviors can emerge by altering contacts. Second, sidewinding is kinematic and it can be

precisely modeled by the mathematical model.

IV. Contact Scheduling

Our observation in biological snakes showed varying positions of body contacts could result in various behaviors. This suggested a similar, bio-inspired strategy for generating useful behaviors on snake robots. Building upon the mathematical model derived in the previous section, we introduce the *contact scheduling* algorithm, which plans positions of body contacts to achieve high-performance gaits for snake robots. In the scope of this work, we only aimed to find gaits that maximally reorient the robot in one gait cycle (turning gaits) using the contact scheduling algorithm.

A close inspection of (10) revealed that the workspace motion of a snake was determined by both contact states, δ, and shape velocities, $\dot{\alpha}$. Considering the many degrees of freedom a snake robot typically has, directly planning in the space of $\dot{\alpha}$ and δ tends to fail because of the formidable computational cost. To overcome the computational barrier and to focus on contact planning, we assumed the shape changes in the horizontal plane, α, were given and the contact scheduling algorithm only needed to specify contacts, δ, throughout a gait cycle. Simultaneously planning shape changes, α, and body contacts, δ, will be discussed in a follow-up paper. We further assumed the body undulations in the horizontal plane was in the form of

$$\alpha(n,t) = \sin(\Omega n + t) \tag{13}$$

where n denoted the joint index, t denoted time (phase) and $\Omega = \frac{2\pi}{N-1}$ was the spatial frequency, which determined the number of waves generated along the snake. This particular choice of α was primarily inspired by Hirose's pioneering work [20] in which he identified the *serpenoid curve* (a curve whose curvature varies sinusoidally along the length) as the fundamental model for undulatory locomotion. The efficacy of using the serpenoid curve in modeling snake locomotions has been independently verified by many groups, including those from the central pattern generator (CPG) community [21], [22] as well as our group [23]. With (13), the shape velocities were readily computed as

$$\dot{\alpha}(i,t) = \cos(\Omega i + t). \tag{14}$$

With known $\dot{\alpha}$, the contact scheduling algorithm only needed to choose contacts, δ, at all phases sampled throughout a gait cycle. Therefore, the goal of the contact scheduling algorithm was to find a sequence of contacts over a time horizon T such that the robot can maximally reorient itself.

A. Contact Space

We start discussion of choosing contacts at one time step. At the beginning of every time interval, the contact scheduling algorithm must choose a contact state, δ, from the *contact space*,

$$\mathcal{C} = \underbrace{\{0,1\} \times \cdots \times \{0,1\}}_{N}, \tag{15}$$

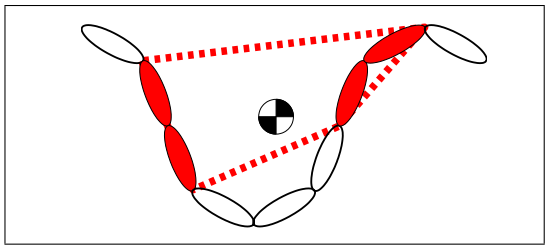

(a) A stable configuration.

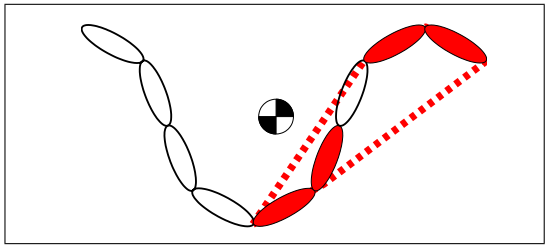

(b) An unstable configuration.

Fig. 4: Illustrations of stable vs. unstable contacts. A link in red means it is in contact. Dashed lines represent the supporting polygons.

defined in a style similar to [24]. For a snake robot with N links, there are $|\mathcal{C}| = 2^N$ different choices of contact states at each time step; $|\mathcal{C}|$ grows exponentially with N. As N gets larger, contact selection quickly become computational infeasible. To mitigate the high computational cost, we made the following simplifying assumption. We assumed a snake made contacts at only two positions along the body and each of the contacts was of length equal to two links according to the observation that biological snakes typically made two body contacts with the substrate during locomotion. This assumption implicitly defined a *simplified contact space*,

$$\tilde{\mathcal{C}} = \{(1,2), \cdots, (N-1,N)\} \times \{(1,2), \cdots, (N-1,N)\},$$

whose size $|\tilde{\mathcal{C}}| = (N-1)^2$. The simplified contact space reduced the computational complexity of choosing contacts at every time step from exponential to polynomial with respect to N. We remark that the simplified contact space, $\tilde{\mathcal{C}}$, potentially compromised the performance of a snake robot because of its restriction on choices of contacts, but it made the contact scheduling computationally feasible.

B. Static Stability Constraint

When deriving the snake model, we assumed the amount of lifting was small and only small motor actuations were required to produce desired contact states. We hence assumed there was no cost in contact transition and the robot could freely transit between all contact states. Nevertheless, some choices of contacts do not satisfy the static stability constraint that the center of mass (CoM) of the system must stay inside the supporting polygon formed by the contacts, as shown in Fig. 4. Inappropriate choices of contact states would cause the robot to tip over and lead to unintended contact states. To ensure the feasibility of the proposed contacts, we eliminated candidate contact states whose convex hull (support polygon) did not enclose the CoM, an approach suggested in [25]. We noted even under this constraint, unintentional contacts

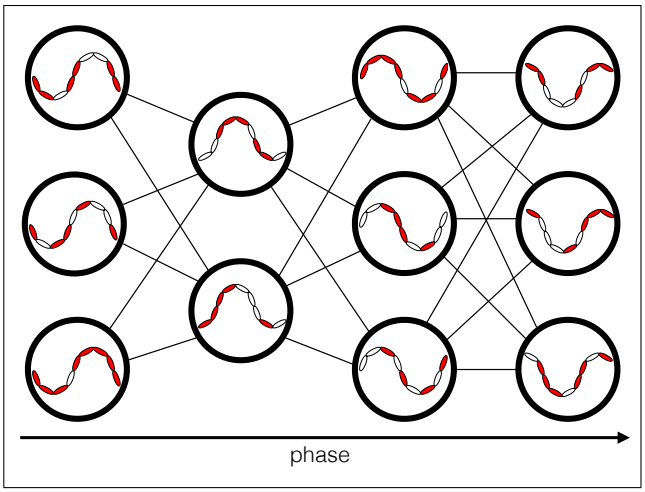

Fig. 5: The schematic of the contact scheduling algorithm. Each circle represents one feasible choice of contact states at one particular time step (phase) in one gait cycle. Circles in the same column denote the contacts at the same time step. Contact states at adjacent time steps are fully connected, denoting a snake can transit to any contact states at the following time step.

occasionally occurred in robot experiments whose impact requires further investigation.

C. Greedy is Optimal

After eliminating all infeasible contact states, the remaining task of the contact scheduling algorithm was to pick contacts at every time step, as depicted in Fig. 5, such that the selected sequence of contacts would result in workspace motion that translate and reorient the snake in a desired manner. However, in the worst case, there was a total of $O\left((N^2)^{(T-1)}\right)$ different sequences of contacts over a time horizon T. It was hence computationally infeasible to find an optimal (maximal net change of orientation per gait cycle) sequence of contacts by naively enumerating all combinations of contacts. To circumvent the high computational cost of straightforward enumeration, we instead proposed a greedy algorithm, which chose contacts that maximize the angular velocity of the head frame in each time interval,

$$\delta^t = \arg\max_{\delta \in \tilde{\mathcal{C}}} \{\nu^t\}, \tag{16}$$

where δ^t denoted the contact state at time step t and ν^t was the angular velocity component in ξ^t_{w0}. It can be shown that, when seeking for gaits that maximally reorient the system (turning gaits), this greedy algorithm actually yields a globally optimal solution.

1) Turn in Place: Turning motion is essential in applications like urban search and research where the robot is required to navigate in confined space. Compared to straight-line sidewinding, turning motion has received far less attention, and theoretical tools to guide the design of turning gaits is lacking. Aided by our contact scheduling algorithm, we were able to design gaits that maximally reorient the snake robot in a gait cycle with given horizontal undulations.

Proof: Define $\Delta\theta^t$ as the net change of orientation of the head frame in time interval t. The objective of the contact scheduling algorithm is to find a sequence of contacts such that the total net change of orientation of the head frame is maximized after one gait cycle,

$$\Delta\theta = \sum_{t=1}^{T-1} \Delta\theta^t. \tag{17}$$

It must be noted that $\Delta\theta$ is invariant to the choice of body reference frame (head frame in this case), because the robot shape returns to its starting configuration after one gait cycle and every segment reorients the same amount. At each time step, our greedy algorithm picks the contact state, δ^t using (16). According to the constant body velocity assumption, the net change of orientation of the head frame in a particular time interval $\Delta\theta^t = \nu^t \Delta t$. The objective of the contact scheduling can hence be written as

$$\Delta\theta^* = \max_{\delta^1,\cdots,\delta^T} \{\sum_{t=1}^{T-1} \Delta\theta^t\}, \tag{18}$$

where $\Delta\theta^*$ is the global optimum of all combinations of contacts. As discussed above, finding an optimal sequence of contacts by enumerating all combinations of $\delta^1, \cdots, \delta^T$ is computationally intractable. However, based on the fact that $\Delta\theta^t$ only depends on δ^t, the following relation holds,

$$\Delta\theta^* \leq \sum_{t=1}^{T-1} \max_{\delta^1,\cdots,\delta^T} \{\Delta\theta^t\} = \sum_{t=1}^{T-1} \max_{\delta^t} \{\Delta\theta^t\}. \tag{19}$$

The right hand side of (19) is exactly the solution to our greedy algorithm, and it upper bounds the global optimum. It can hence be concluded that the proposed greedy algorithm actually yields the globally optimal solution for turning. ■

V. Results

Figure. 6 shows the contact pattern associated with the optimal turning gait resulting from the contact scheduling algorithm. In simulation, the this gait reoriented the snake $\approx 100^\circ$ in one gait cycle. Implementing this gait on a snake robot resulted in a remarkable turning gait superior to any gait that has previously reported in terms of agility, defined as the number of gait cycles required to rotate 360°, and maneuverability, defined as the radius of the minimal enclosing circle of the CoM trajectory after the robot rotated 360°.

A. The Unified Snake Robot

We used the *unified snake robot* [26] (Fig. 1(b)) as the platform to examine the efficacy of the contact scheduling algorithm. The unified snake robot is a serial chain of 16 identical links, each of which provides one DoF. These joints rotate alternatively in the dorsal and lateral planes such that the robot can deform into three-dimensional shapes.

The structure of the unified snake robot is not completely identical to the mathematical model described in the previous section. The model assumed universal joints between segments, while the joints of the unified snake robot are pitch-yaw connected. To account for the difference, we abstracted every pair of pitch-yaw joints in the unified snake robot as if it were one segment which can rotate in both pitch

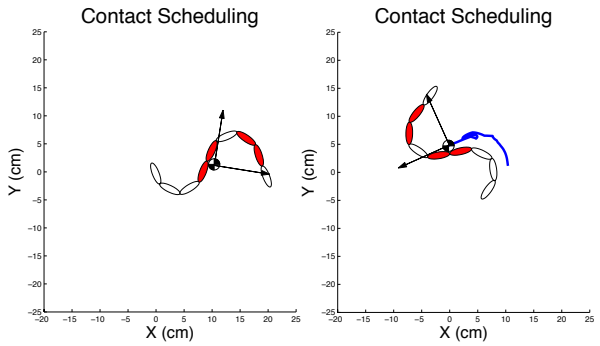

(a) Initial configuration. (b) Terminal configuration.

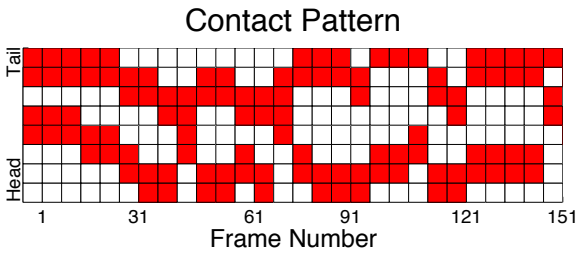

(c) Contact pattern of the turning gait.

Fig. 6: The simulated result and the corresponding contact patterns associated with the turning gait resulting from the contact scheduling algorithm. The simulated snake reoriented $\approx 100^\circ$ in one gait cycle. The blue line in Fig. 6(b) denotes the trajectory of CoM.

(vertical) and yaw (horizontal) direction, in a manner similar to a universal joint.

B. Contact Policy

The contact scheduling algorithm planned for contact patterns, but did not generate joint inputs to instantiate the planned contacts. To achieve the desired contact states on the unified snake robot, a mapping, termed a *contact policy*, from the designated contacts to corresponding joint angles was required. Contact policies were not unique. Different heights of lifting would result in different joint motions, but achieve the same contact states. For simplicity and to satisfy the requirement that the amount of lifting remain small, we designed our contact policy as follows. As shown in Fig. 7, for a segment in contact, we set the heights of its proximal and distal joints to be 0 and the heights of the rest of the joints to be Δh. Using the small angle approximation, the pitch angle of a particular segment, β_i, was computed as

$$\beta_i = \sin^{-1}\left(\frac{h_i - h_{i-1}}{L}\right) \approx \frac{h_i - h_{i-1}}{L}, \qquad (20)$$

where L was the length of a segment. The internal joint angle α_i between the two segments, $i-1$ and i, was then be computed as

$$\alpha_i = \beta_i - \beta_{i-1} = \frac{h_i - 2h_{i-1} + h_{i-2}}{L}. \qquad (21)$$

It must be noted that there existed contact states that were physically infeasible. As shown in Fig. 7(b), when the middle link was supposed to lift off the ground while both of its

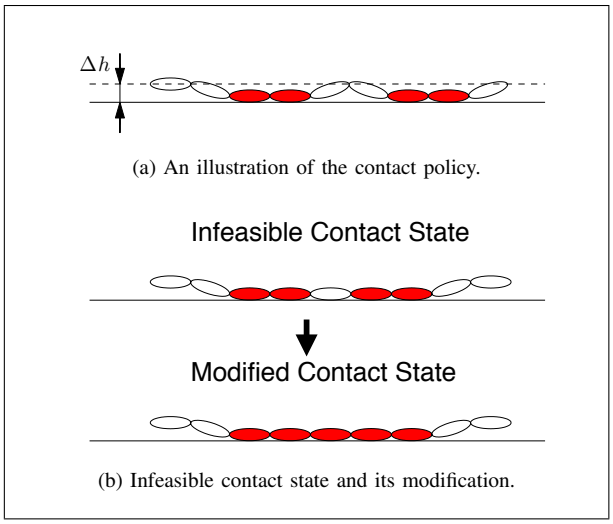

(a) An illustration of the contact policy.

(b) Infeasible contact state and its modification.

Fig. 7: An illustration of the contact policy and an infeasible contact state. Links in red means they are in contact with the ground.

neighbors were in contact, due to the insufficient DoFs in the dorsal plane, the middle link had to touch the ground. In this case, we simply modified the planed contact states according to the strategy depicted in Fig. 7(b).

C. Robot Experiments

Equation (13) specified control inputs for the horizontal joints and the contact policy generated control inputs for the vertical joints. Entering the joint trajectories to the unified snake robot resulted in a turn in place motion that reoriented the snake robot $103.2 \pm 22.5^\circ$ (average of 30 robot experiments) in a gait cycle, as shown in Fig. 8(b). We compared its performance with the state-of-art turning gait, *conical sidewinding* [23], in terms of agility and maneuverability. Fig. 8 shows the novel turn in place motion outperformed the conical sidewinding more than 100% in both agility and maneuverability. This type of fast and tight turning motion would benefit applications such as urban search and rescue, where the robot has to navigate in confined environments.

VI. Conclusions and Future Work

Our studies in biological snakes together with robot experiments emphasize the fundamental importance of the vertical undulation in terrestrial limbless locomotion. Both biological snakes and robots can change the positions of contacts via vertical undulation to produce distinct behaviors. The results presented in this paper not only explained the various behaviors observed in biological snakes, but also brought valuable engineering insights for designing better gaits for snake robots. These insights led to the proposal of the contact scheduling algorithm, which horizontal and vertical undulations in a decoupled fashion. Separately considering undulations in the horizontal and vertical planes not only simplifies computation but is a more principled way to consider limbless locomotions involving three-dimensional body undulations. Although this paper focused on snake robots, the contact scheduling algorithm introduces a powerful motion generation framework for locomotors that can make and break contacts with the ground.

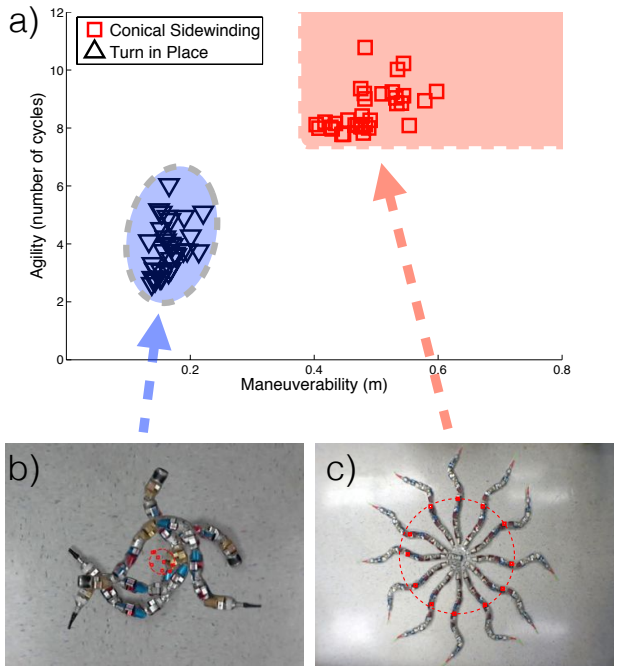

Fig. 8: The comparison of performance between the novel turn in place motion versus the conical sidewinding gait. Insets b) and c) illustrate how maneuverability was measured.

This work introduces a principled way to view the horizontal and vertical body undulations in three-dimensional limbless locomotion. Although this paper has focused on scheduling contacts by utilizing vertical motion, the presented methodology can be further extended to consider the interplay between the horizontal and vertical motions. Extensions to the contact scheduling that simultaneously plan motions in the horizontal and vertical planes would capture a larger set of motions and could potential lead to more capable gaits. Simultaneously planning horizontal and vertical motions will be discussed in a follow-up paper. This paper focused on turning gaits, but the presented planning diagram, as depicted in Fig. 5, is general. Previously established graph search algorithms can be readily employed for designing gaits other than turning using this paradigm.

References

[1] W. Mosauer, "A Note on the Sidewinding Locomotion of Snakes," *The American Naturalist*, vol. 64, no. 691, pp. 179–183, March 1930.

[2] H. Marvi, C. Gong, N. Gravish, H. C. Astley, M. Travers, R. Hatton, J. R. M. III, H. Choset, D. L. Hu, and D. I. Goldman, "Sidewinding with minimal slip: snake and robot ascent of sandy slopes," *Science, in press*, 2014.

[3] P. Liljebäck, K. Y. Pettersen, Ø. Stavdahl, and J. T. Gravdahl, "Snake robots: Modelling, mechatronics, and control," 2012.

[4] D. L. Hu, J. Nirody, T. Scott, and M. J. Shelley, "The mechanics of slithering locomotion," *Proceedings of the National Academy of Sciences*, vol. 106, no. 25, pp. 10 081–10 085, 2009.

[5] A. J. Ijspeert and A. Crespi, "Online Trajectory Generation in an Amphibious Snake Robot Using a Lamprey-like Central Pattern Generator Model," in *IEEE Conference on Robotics and Automation*, 2007.

[6] C. Gong, R. Hatton, and H. Choset, "Conical sidewinding," in *Robotics and Automation (ICRA), 2012 IEEE International Conference on*, may 2012, pp. 4222 –4227.

[7] I. Tanev, T. Ray, and A. Buller, "Automated evolutionary design, robustness, and adaptation of sidewinding locomotion of a simulated snake-like robot," *Robotics, IEEE Transactions on*, vol. 21, no. 4, pp. 632–645, 2005.

[8] C. Ye, S. Ma, B. Li, and Y. Wang, "Turning and side motion of snake-like robot," in *Robotics and Automation, 2004. Proceedings. ICRA'04. 2004 IEEE International Conference on*, vol. 5. IEEE, 2004, pp. 5075–5080.

[9] P. Domenici and R. Blake, "The kinematics and performance of fish fast-start swimming," *Journal of Experimental Biology*, vol. 200, no. 8, pp. 1165–1178, 1997.

[10] B. C. Jayne, "Kinematics of terrestrial snake locomotion," *Copeia*, pp. 915–927, 1986.

[11] H. Astley, C. Gong, M. Travers, M. Serrano, P. Vela, H. Choset, J. Mendelson, D. Hu, and D. Goldman, "Modulation of orthogonal body waves enables high maneuverability in sidewinding locomotion," *Proceedings of the National Academy of Sciences*, 2014.

[12] J. Burdick, J. Radford, and G. Chirikjian, "A "Sidewinding" Locomotion Gait for Hyper-redundant Robots," *Robotics and Automation*, vol. 3, pp. 101–106, 1993.

[13] R. D. Maladen, Y. Ding, C. Li, and D. I. Goldman, "Undulatory swimming in sand: subsurface locomotion of the sandfish lizard," *science*, vol. 325, no. 5938, pp. 314–318, 2009.

[14] J. Gray, "The Mechanism of Locomotion in Snakes," *Journal of Experimental Biology*, vol. 23, no. 2, pp. 101–123, December 1946.

[15] S. Kelly and R. M. Murray, "Geometric Phases and Robotic Locomotion," *J. Robotic Systems*, vol. 12, no. 6, pp. 417–431, Jan 1995.

[16] J. Avron and O. Raz, "A geometric theory of swimming: Purcell's swimmer and its symmetrized cousin," *New Journal of Physics*, vol. 9, no. 437, 2008.

[17] R. L. Hatton and H. Choset, "Geometric swimming at low and high reynolds numbers," *Robotics, IEEE Transactions on*, vol. 29, no. 3, pp. 615–624, 2013.

[18] R. M. Murray, Z. Li, and S. S. Sastry, *A Mathematical Introduction to Robotic Manipulation*. CRC Press, 1994.

[19] C. W. Wampler, "Manipulator inverse kinematic solutions based on vector formulations and damped least-squares methods," *Systems, Man and Cybernetics, IEEE Transactions on*, vol. 16, no. 1, pp. 93–101, 1986.

[20] S. Hirose, *Biologically Inspired Robots (Snake-like Locomotor and Manipulator)*. Oxford University Press, 1993.

[21] J. Gonzalez-Gomez, H. Zhang, E. Boemo, and J. Zhang, "Locomotion Capabilities of a Modular Robot with Eight Pitch-Yaw-Connecting Modules," in *9th International Conference on Climbing and Walking Robots.*, 2006.

[22] A. J. Ijspeert, "Central Pattern Generators for Locomotion Control in Animals and Robotics," *Neural Networks*, vol. 21, pp. 642–653, 2008.

[23] C. Gong, M. J. Travers, X. Fu, and H. Choset, "Extended gait equation for sidewinding," *Robotics and Automation (ICRA), 2013 IEEE International Conference on*, 2013.

[24] A. M. Johnson and D. E. Koditschek, "Toward a vocabulary of legged leaping," in *Robotics and Automation (ICRA), 2013 IEEE International Conference on*. IEEE, 2013, pp. 2568–2575.

[25] M. Tanaka and F. Matsuno, "Modeling control of a snake robot with switching constraints," in *SICE Annual Conference, 2008*. IEEE, 2008, pp. 3076–3079.

[26] C. Wright, A. Buchan, B. Brown, J. Geist, M. Schwerin, D. Rollinson, M. Tesch, and H. Choset, "Design and architecture of the unified modular snake robot," in *Robotics and Automation (ICRA), 2012 IEEE International Conference on*. IEEE, 2012, pp. 4347–4354.